A Battery Balancing Auxiliary Power Module with Predictive Control for Electrified Transportation

Matthias Preindl, *Member, IEEE*

***Abstract*—This research proposes the integration of the auxiliary power module (APM) and nondissipative balancing hardware of a high-voltage battery. The proposed battery-balancing APM is projected to reduce the costs of nondissipative battery balancing by providing two functionalities: balancing of the high-voltage battery cells and charging of the low-voltage battery. This research proposes two model predictive control (MPC) strategies that address simultaneous balancing and charging. Both approaches make unbalanced charge available that increases the effective capacity of the high-voltage battery. The monolithic controller solves the balancing and charging problem as a single optimization problem. In contrast, the decoupled controller defines a separate control law for charging to achieve a higher bandwidth, e.g. for systems without dedicated low-voltage battery. The battery-balancing APM concept is validated on a software-in-the-loop and experimental test bench.**

***Index Terms*—Auxiliary power module, batteries, battery balancing, charge transfer, DC-DC power conversion, electric vehicle, energy storage system, optimal control, predictive control, power electronics**

I. Introduction

ELECTRIC vehicles (EV) and plug-in hybrid electric vehicles (HEV), are moving towards drivetrains with high-power electric machines and inverters. These drivetrains require energy storage systems with high voltage, high efficiency, and long lifetime [1], [2]. High voltage levels are achieved connecting battery (or supercapacitor) cells in series. The capacity of the stacked cells tends to differ due to internal (internal impedance and different self-discharge rate) and external (temperature variations) effects [3]. Hence, the charge and discharge rates vary across the stack and result in charge imbalances that worsen over time. A battery management system (BMS) checks each cell for over and undercharging. Otherwise, the cell life reduces nearly exponentially with the string length [4], [5]. In addition, the state-of-charges (SOC) of the cells need to be equalized repeatedly to avoid that a stack contains cells with both low and high SOC and only a fraction of the capacity can be used [6].

There are two types of balancing operation: *balancing* and *redistributive-balancing* (or simply *redistribution*). Balancing equalizes the cell SOC typically during charging. Using balancing, a stack can only be discharged until the cell with the smallest capacity is empty. In other words, the effective capacity of the stack is $Q_{\text{eff}} = \min[Q_1, \ldots, Q_n]'$ for balancing [6], where $Q_1, \ldots, Q_n$ are the cell capacities and $'$ is the transposition operator. Redistribution continuously equalizes the cell SOC and avoids that smaller cells are depleted by moving charge between cells. Hence, redistribution makes excess charge of high-capacity cells available, i.e. it increases the effective capacity of the stack that is $Q_{\text{eff}} = \text{mean}[Q_1, \ldots, Q_n]'$ [6]. Furthermore, it can be argued that redistribution increases the reliability and lifetime of a battery pack since a single or few bad cells have a limited effect on the effective capacity [6], [7]. Hence, redistribution has strong benefits over "conventional" balancing but requires balancing links with a higher current rating to maintain a balanced stack [6].

Two classes of hardware are used for balancing: *dissipative* and *nondissipative*. In dissipative balancing, excess charge is drawn from the cells with the highest SOC and is dissipated through shunt resistors or transistors [3]. Redistribution requires nondissipative hardware that uses power electronic links to move charge between cells [8], [9]. Nondissipative balancing is significantly more energy efficient, i.e. it achieves a significantly lower *energy-loss-to-balance* (e2b), and can achieve the same performance, i.e. *time-to-balance* (t2b), compared to dissipative balancing [10]. In practice, EV manufactures hesitate to implement nondissipative (redistributive or "classic") balancing due to cost [2]. The realization of inexpensive hardware is challenging due to the system complexity (sensors, local controllers, etc.) and the cumulative power rating of the links (typically several kW for redistribution [6]).

This paper studies the integration of a nondissipative battery-balancing hardware with the auxiliary power module to mitigate the cost issue. The resulting *battery-balancing* APM (BB-APM) is based on the capacitive storage element topology that has been shown to be among the best performing topologies in terms of time-to-balance and energy-loss-to-balance [10]. The proposed topology provides two functionalities: balancing of the high-voltage battery cells and charging of the low-voltage battery. The topology can be implemented with a "classic" balancing strategy, where balancing is performed exclusively when the high-voltage battery is charged. This approach simplifies the control since it is limited to supply power to the auxiliary system when the vehicle is in operation. However, a typical APM power rating is $\sim$ 3kW [11]–[13] that is in line with requirements for redistributive balancing. Hence, this research studies simultaneous balancing and charging. Two model predictive control (MPC) strategies are proposed. The monolithic controller solves the balancing and charging problem as a single optimization problem. The decoupled controller defines a separate control law for charging to achieve a

Manuscript received October 3, 2016; revised January 1, 2017 and January 23, 2017; accepted February 13, 2017.

M. Preindl is with the Department of Electrical Engineering, Columbia University, New York, USA (phone: 212-853-0791; fax: 212-932-9421; e-mail: matthias.preindl@columbia.edu)

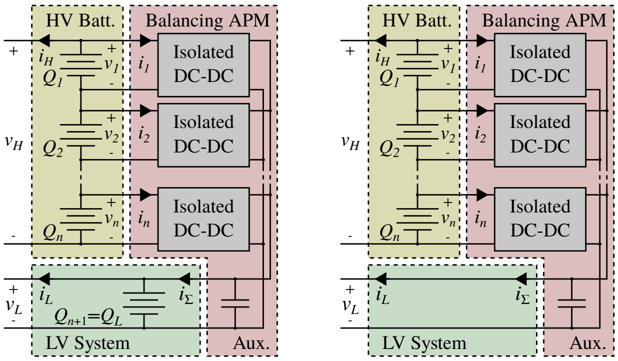

(a) With LV battery (b) Without LV battery

Fig. 1. Battery-balancing APM with high-voltage (HV) and low-voltage (LV) bus, isolated uni-, or bidirectional links, and with, or without LV battery

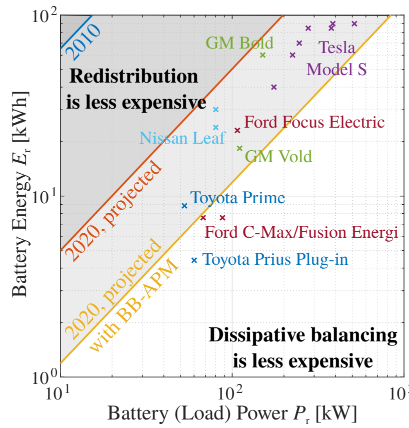

Fig. 2. Cost comparison of dissipative balancing and redistribution: the gray areas highlight where redistribution is less expensive than dissipative balancing using 2010 data and projected 2020 data with conventional drivetrain and with BB-APM

higher bandwidth, e.g. for systems without or small dedicated low-voltage battery.

Block diagrams of the proposed BB-APM are shown in Fig. 1 with different low-voltage system configurations. The main battery consists of series connected battery modules that are connected to the high-voltage (HV) DC bus. Each module can contain one or more series and/or parallel connected battery cells. Isolated DC-DC converters form the balancing links that are either unidirectional or bidirectional. They are connected to a battery on the isolated low-voltage (LV) DC bus. In EVs, typical voltages are 200V to 800V for the HV bus and 12V, 24V, or 48V for the LV bus. In addition, the BB-APM can be modularized by grouping more than one DC-DC converter and the control electronics. The BB-APM concept is validated by a software-in-the-loop (SiL) and experimental test bench using a reconfigured Linear Technology DC2100A board.

II. Cost Analysis

The cost of dissipative balancing and redistribution is compared using a back-of-the-envelope calculation [6] that is adapted for the BB-APM concept. Given cells with a typical capacity Q_{eff} and the capacity tolerance $\pm Q_\Delta$ (or relative tolerance $\pm q_\Delta = Q_\Delta / Q_{\text{eff}}$), a "classically" balanced stack requires cells with capacity $Q_{\text{eff}} + Q_\Delta$ to realize a stack with capacity Q_{eff}. A stack with redistribution uses cells with capacity Q_{eff} but needs to compensate Q_Δ by moving charge over the links. Therefore, balancing is advantageous for low-energy, high-power packs and redistribution is advantageous for high-energy, low-power packs.

The limit where one method is beneficial over the other is estimated calculating the cost of the energy storage system C_{ess} as shown in Table I. The cost of the cells is computed using the specific battery cost c_{cel} (in \$/kWh) and the total installed energy storage capacity E_{cel}. The cost of the battery balancing hardware is computed from the specific cost of the power electronics c_{bal} (in \$/kW) and the cumulative power rating of all balancing links P_{bal}. The cost of a discrete APM is obtained from the specific cost of an APM c_{bal} (in \$/kW) and its power rating P_{apm}. A comparison of the costs is obtained putting these values into perspective for a battery pack with rated energy storage E_r and power P_r. A "classically" balanced stack requires an extra energy storage of $q_\Delta E_{\text{r}}$ and a stack with redistribution requires redistributive hardware with power $q_\Delta P_{\text{r}}$ [6]. Compared to redistribution, dissipative balancing requires a lower power rating and each link is simpler, i.e. cheaper [6]. For simplicity, the cost of the dissipative balancing hardware is neglected, which is optimistic for the dissipative balancing costs. Using a BB-APM, the APM functionality is provided by the redistributive balancing hardware and a discrete APM is not required.

The costs are compared in Fig. 2 by plotting the limits where redistribution is less expensive than dissipative balancing. It is shown that redistribution becomes more cost competitive in 2020 as compared to 2010 but dissipative balancing remains preferable for vehicle drivetrains. The proposed BB-APM is projected to shift the balance in favor of redistribution making it competitive for EVs and some HEVs. A final cost assessment of a BB-APM design requires implementation details and corporate cost datas. However, the projection suggests a consideration of the BB-APM concept for future EV designs.

III. System Model

This research focuses on the energy storage system shown in Fig. 1. It consists of a HV battery (or supercapacitor) pack with n energy storage elements that are connected in series. The $n+$ 1-th energy storage element is connected to a galvanic isolated

Table I
Battery Pack Cost Model

	dissip. bal.	nondissip. bal.	BB-APM
Total cost C_{ess}	$c_{\text{cel}}E_{\text{cel}} + c_{\text{bal}}P_{\text{bal}} + c_{\text{apm}}P_{\text{apm}}$		
Installed energy storage E_{cel}	$(1+q_\Delta)E_{\text{r}}$	E_{r}	E_{r}
Balancing link power P_{bal}	~ 0W	$q_\Delta P_{\text{r}}$	$q_\Delta P_{\text{r}}$
Power of discrete APM P_{apm}	$p_{\text{apm}}P_{\text{r}}$	$p_{\text{apm}}P_{\text{r}}$	0W

Fig. 2 uses 2010 data from [6], the 2020 power electronic target \$50/kW for isolated DC-DC converters [11] (a 200% cost penalty is added for redistributive links due to the lower power rating per link), and battery cost projection \$200/kWh for 2020 [14]. The figure is drawn for the conditions: $q_\Delta = 5\%$ and the relative APM power $p_{\text{apm}} = 5\%$.

LV bus. Each element is either a single cell or a module with multiple cells connected in parallel and/or series. The j-th element of the stack contains the charge $Q_j x_j[k]$, where $Q_j \in \mathbb{R}_{>0}$ is the rated capacity, $x_j[k] \in \mathbb{R}_{\geq 0}$ is the SOC, and $k \in \mathbb{N}_{\geq 0}$ specifies the discrete sampling instant kT_s where T_s is the sampling period. A battery cell stores, i.e. provides, the charge that flows in its terminals. Hence, the SOC of the HV cells evolves according to [10], [15]

$$x_j[k+1] = x_j[k] - \frac{T_s}{Q_j}\left(i_j[k] + i_H[k]\right), \tag{1}$$

where $i_H[k] \in \mathbb{R}$ is the current provided to the HV link and $i_j[k] \in \mathbb{R}$ is the balancing current in the j-th cell as shown in Fig. 1. Similar, the SOC of the LV side evolves according to

$$x_L[k+1] = x_L[k] + \frac{T_s}{Q_j}\left(i_\Sigma[k] - i_L[k]\right), \tag{2}$$

where $i_L[k] \in \mathbb{R}$ is the current provided to the LV link and $i_\Sigma[k] \in \mathbb{R}$ is the LV side current created by all balancing links. The balancing currents $i_j[k]$ are generated by isolated DC-DC converters that are modeled as ideal DC-transformers for control purposes. Each balancing link generates the current $\frac{V_j}{V_L} i_j[k]$ on its LV side, where V_j is the voltage of the j-th HV cell and V_L is the voltage of the LV link. The LV link is charged by each link that results in

$$i_\Sigma[k] = \sum_{j=1}^{n} \frac{V_j}{V_L} i_j[k]. \tag{3}$$

The current $i_\Sigma[k]$ depends on the cell voltages $V_j \in \mathbb{R}_{>0}$. In practice, these voltages are well known, i.e. measured, and tend to vary only within limited intervals. Hence, the transformation ratios $\frac{V_j}{V_L}$ are treated as system parameters that are assumed to be constant within at least one sampling period.

An energy storage system with BB-APM can be described dynamically in matrix form. The dynamic model is obtained combining (1) of all HV cells and (2)

$$x[k+1] = x[k] + \mathbf{B}u[k] + \mathbf{E}w[k], \tag{4}$$

that is a generalization of the models used in [10], [15], [16]. The dynamic model is written in state-space form, where the state is the SOC vector

$$x[k] = [x_1[k], \ldots, x_j[k], \ldots, x_n[k], x_L[k]]' \in \mathbb{R}^{n+1}_{\geq 0}. \tag{5}$$

In practice, the SOC's cannot be measured directly but estimated using cell models [17], [18]. Throughout this text, the SOC of each element is assumed to be known, i.e. estimated with sufficient precision, e.g. using [19]–[22]. The (controlled) input is the vector of HV-side balancing link currents

$$u[k] = [i_1[k], \ldots, i_j[k], \ldots, i_n[k]]' \in \mathbb{R}^n. \tag{6}$$

The input matrix is defined by $\mathbf{B} = T_s \mathbf{Q}^{-1}\mathbf{T} \in \mathbb{R}^{(n+1)\times n}$, where $\mathbf{Q} = \operatorname{diag}[Q_1, \ldots, Q_n, Q_L]' \in \mathbb{R}^{(n+1)\times(n+1)}$. The topology matrix $\mathbf{T}$ describes a connected graph and defines how the links connect the elements with each other and the LV bus [10], [16]. The proposed BB-APM topology is obtained connecting each HV element to the LV bus. Using the convention that the current is positive when it flows from the HV to the LV side, the topology matrix is

$$\mathbf{T} = \begin{bmatrix} -1 & 0 & \ldots & 0 \\ 0 & -1 & \ldots & 0 \\ \vdots & \vdots & & \vdots \\ 0 & 0 & \ldots & -1 \\ \frac{V_1}{V_L} & \frac{V_2}{V_L} & \ldots & \frac{V_n}{V_L} \end{bmatrix} \in \mathbb{R}^{(n+1)\times n}. \tag{7}$$

The current drawn from the HV and LV link are imposed externally and act as exogenous input, i.e. known disturbance

$$w[k] = [i_H[k], i_L[k]]'. \tag{8}$$

The effect of $w[k]$ is described by $\mathbf{E} = T_s \mathbf{Q}^{-1}\bar{\mathbf{T}}$, where

$$\bar{\mathbf{T}} = \begin{bmatrix} -1_n, 0_n \\ 0, -1 \end{bmatrix} \in \mathbb{R}^{(n+1)\times 2}, \tag{9}$$

is the matrix that links the LV and HV stack current with the cells where it flows. The SOC, link currents, and stack currents are constrained to avoid damage of the cells and links

$$x[k] \in \mathcal{X}, \;\; u[k] \in \mathcal{U}, \;\; w[k] \in \mathcal{W}. \tag{10}$$

We define a cell to be empty when $x_j[k] = 0$ and full when $x_j[k] = 1$. Hence, the state constraint is $\mathcal{X} = [0,1]^{n+1}$ [10], [16]. The link current defines how much power is transferred over a link and needs to be limited according to the minimum rated current $I_{k,\text{min}}$ and maximum rated current $I_{k,\text{max}}$ that results in the input constraint set

$$\mathcal{U} = \{ i \subseteq \mathbb{R}^n \mid I_{j,\text{min}} \leq i_j \leq I_{j,\text{max}} \; \forall j \in \{1, \ldots, n\}\}. \tag{11}$$

If a converter is unidirectional, the minimum current is zero, i.e. $I_{k,\text{min}} = 0$. It is possible to add other constraints, e.g. the power that is transferred over a link or the total balancing currents to prevent the stack from overheating [10], [16]. The known disturbance $w[k]$ is imposed externally and it is assumed that both $i_H[k]$ and $i_L[k]$ are limited externally such that they satisfy the maximum discharge ($I_{H,\text{max}}$, $I_{L,\text{max}}$) and charge ($I_{H,\text{min}}$, $I_{L,\text{min}}$) current [23], i.e.

$$\mathcal{W} = \left\{ w \subseteq \mathbb{R}^2 \mid \begin{bmatrix} I_{H,\text{min}} \\ I_{L,\text{min}} \end{bmatrix} \leq \begin{bmatrix} i_H \\ i_L \end{bmatrix} \leq \begin{bmatrix} I_{H,\text{max}} \\ I_{L,\text{max}} \end{bmatrix} \right\}. \tag{12}$$

A $w[k] \neq 0_2$ tends to discharge the LV element and unbalance the HV stack during discharge and balance the stack during charging operation due to capacity Q_j differences across the stack. The effect of $w[k]$ is linear and balancing hardware as well as chargers are typically studied invoking the superposition principle. Balancing systems are studied on an unbalanced HV stack with $i_H = 0$A [24]–[27] and APM are studied on a discharged LV cell for $i_L = 0$A [12], [13], [28]. In this research, the term $w[k]$ is kept throughout the analytical treatment but testing is performed for $w[k] = 0_2$ for compactness and clearness of the results.

IV. Balancing and Power Supply Problem

The energy storage system is said to have a *balanced* HV subsystem when all its n HV elements have the same SOC

$$x[k] \in \mathcal{X}_b = \left\{ x \in \mathbb{R}^{n+1} \mid x_j = x_k \; \forall j, k \in \{1, \ldots, n\} \right\}. \tag{13}$$

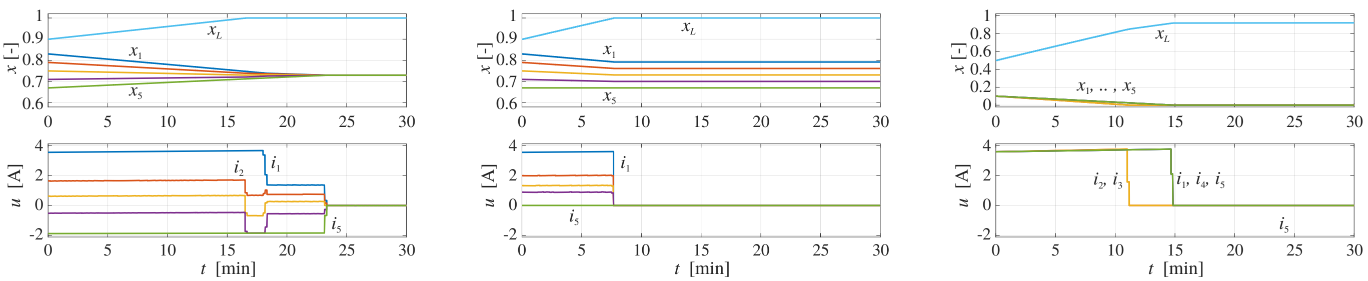

(a) Feasible balancing with bidirectional links (b) Infeasible balancing with bidirectional links (c) Infeasible charging with empty HV battery

Fig. 3. Examples of balancing and charging feasibility: balancing with bidirectional links is always feasible; balancing with unidirectional links is infeasible once the LV is fully charged; charging is infeasible once the HV elements are fully discharged

The HV elements transfer energy to the isolated LV element acting as APM. The LV element is said to be *charged* if

$$x[k] \in \mathcal{X}_c = \left\{ x \in \mathbb{R}^{n+1} \mid x_{n+1} = x_L = 1 \right\}. \tag{14}$$

The HV system is balanced and the LV element is charged if $x[k] \in \mathcal{X}_b \cap \mathcal{X}_c$. The statement $x[k] \in \mathcal{X}_b$ is simplified introducing the unbalanced SOC of the HV cells. The unbalanced SOC is the cell SOC minus the average HV stack SOC [10]

$$\bar{x}_j[k] = x_j[k] - \frac{1}{n} \sum_{l=1}^{n} x_l[k]. \tag{15}$$

This concept is used to introduce the affine transformation

$$\tilde{x}[k] = \mathbf{L}x[k] - r. \tag{16}$$

The linear transformation $\mathbf{L}x[k]$ results in a vector that contains the unbalanced SOC of the HV cells on the first n components and the the LV SOC on the last component. The matrix is defined by

$$\mathbf{L} = \begin{bmatrix} \mathbf{I}_n - \frac{1}{n}\mathbf{1}_n & 0_n \\ 0_n' & 1 \end{bmatrix} \in \mathbb{R}^{(n+1)\times(n+1)}, \tag{17}$$

where $\mathbf{I}_n$ denotes the $n \times n$ identity matrix and $\mathbf{1}_n$ is the $n \times n$ matrix of ones. The vector r defines the balancing and charging goals: zero unbalanced SOC and a fully charged LV cell, i.e. $r = [0, \ldots, 0, 1]' \in \mathbb{R}^{n+1}$. Finally, the vector $R = [0, \ldots, 0, 1]' \in \mathbb{R}^{n+1}$ and the matrix $\mathbf{R} = \operatorname{diag} R$ extract the charging term setting the balancing components to zero.

Proposition 1 (Charged LV element)**.** *A $x[k] \in \mathcal{X}_c$ if and only if $\boldsymbol{R}\tilde{x}[k] = 0_{n+1}$.*

Proof. The vector $\theta = \mathbf{R}\tilde{x}[k]$ is independent of the SOC of the HV elements since $\theta_j = 0$ for all $j \in \{1, \ldots, n\}$ and $\theta_{n+1} = x_L[k] - 1$. Hence $\theta = 0_{n+1}$ implies that $x_L[k] = 1$, i.e. $x[k] \in \mathcal{X}_c$. Also, $\theta_{n+1} \neq 0$ implies $x[k] \notin \mathcal{X}_c$. □

Similarly, the matrix $\bar{\mathbf{R}} = \mathbf{I}_{n+1} - \mathbf{R}$ extract the balancing components setting the charging term to zero.

Proposition 2 (Balanced HV elements)**.** *A $x[k] \in \mathcal{X}_b$ if and only if $\bar{\boldsymbol{R}}\tilde{x}[k] = 0_{n+1}$.*

Proof. The vector $\phi = \bar{\mathbf{R}}\tilde{x}[k]$ is independent of the SOC of the LV element $x_L[k]$ since $\phi_{n+1} = 0$. The components $\phi_j = \tilde{x}_j[k]$ for all $j \in \{1, \ldots, n\}$. Hence $\phi = 0_n$ implies that all HV elements have the same SOC, i.e. $x[k] \in \mathcal{X}_b$. Also, if there exist a $\phi_j \neq 0$ then $x[k] \notin \mathcal{X}_b$. □

Combining both results, $\tilde{x}[k] = 0_{n+1}$ implies that the LV element is charged and the HV elements are balanced, i.e. $x[k] \in \mathcal{X}_b \cap \mathcal{X}_c$. The affine transformation (16) is used to update the dynamic model multiplying (4) with $\mathbf{L}$ and subtracting r

$$\tilde{x}[k+1] = \tilde{x}[k] + \tilde{\mathbf{B}}u[k] + \tilde{\mathbf{E}}w[k], \tag{18}$$

where $\tilde{\mathbf{B}} = \mathbf{LB} \in \mathbb{R}^{(n+1)\times n}$ and $\tilde{\mathbf{E}} = \mathbf{LE} \in \mathbb{R}^{(n+1)\times 2}$. The model (18) translates the balancing and charging problem into a regulation problem with the following property.

Proposition 3 (Stabilizability of the unconstrained system)**.** *There exists an input $u \in \mathbb{R}^n$ such that $x[\tau] \in \mathcal{X}_b$ and $x[\tau] \in \mathcal{X}_c$ with $\tau \in \mathbb{N}_{\geq 0}$ for any initial state $x(0) \in \mathcal{X}$.*

Proof. The transformation (17) contains a redundant state. The HV system is balanced if the SOC difference between each neighbor cells is zero. We introduce

$$\bar{\mathbf{L}} = \begin{bmatrix} 1 & -1 & 0 & \ldots & 0 & 0 & 0 \\ 0 & 1 & -1 & \ldots & 0 & 0 & 0 \\ \vdots & \vdots & \vdots & & \vdots & \vdots & \vdots \\ 0 & 0 & 0 & \ldots & 1 & -1 & 0 \\ 0 & 0 & 0 & \ldots & 0 & 0 & 1 \end{bmatrix} \in \mathbb{R}^{n\times(n+1)}, \tag{19}$$

such that the system is balanced and charged if and only if $\bar{\mathbf{L}}\tilde{x}[k] = 0_n$. The unconstrained feedback controller $u[k] = -\mathbf{K}(\bar{\mathbf{L}}\tilde{x}[k])$ yields the close loop dynamics

$$\bar{\mathbf{L}}\tilde{x}[k+1] = \left(\mathbf{I}_n - \bar{\mathbf{L}}\tilde{\mathbf{B}}\mathbf{K}\right)\bar{\mathbf{L}}\tilde{x}[k] + \bar{\mathbf{L}}\tilde{\mathbf{E}}w[k]. \tag{20}$$

The matrix $\bar{\mathbf{L}}\tilde{\mathbf{B}}$ has full rank n that implies the existstence of a controller $\mathbf{K} \in \mathbb{R}^{n\times n}$ such that all eigenvalues of $\mathbf{I}_n - \bar{\mathbf{L}}\tilde{\mathbf{B}}\mathbf{K}$ are negative. Hence, there exists a feedback controller that yields a stable closed loop system. □

The above result states that the balancing and charging problem is always feasible for the unconstrained system. In practice, the inputs, i.e. balancing currents, are limited due to cost. In particular, hardware, which is not rated for redistribution, can achieve the regulation goals only over time, e.g. when $w[k]$ tends to zero. Furthermore, Proposition 3 does not imply that $x[\tau] \in \mathcal{X}$. This can affect the feasibility of the regulation goals and some examples are shown in Fig. 3. Bidirectional links ($I_{j,\min} < 0$A) can move charge between the

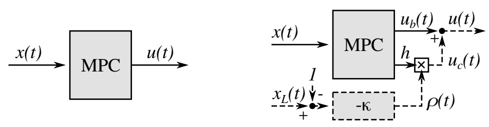

(a) Monolithic Control (b) Decoupled Control

Fig. 4. Control concepts: monolithic control solves the charging and balancing problem as a single MPC; decoupled control separates the problems and the charging control (dashed path) can be executed at higher sampling frequencies

HV cells. Hence, balancing is always feasible as it is shown in Fig. 3(a). Unidirectional links ($I_{j,\text{min}} = 0\text{A}$) balance the HV cells by moving charge to the LV element. Hence, balancing is only feasible if the LV element is not fully charged[1], as it is shown in Fig. 3(b). Similarly, charging is only feasible if the HV cells contain sufficient energy, which is shown in Fig. 3(c).

V. Control

In this section, we show two reference control implementations for the BB-APM. Both balancing and charging can be addressed with a single constrained multi-input multi-output controller. This approach is named *monolithic* control and is depicted in the block diagram Fig. 4(a). We address this problem using MPC that solves a constrained finite time optimal control problem (CFTOC) at each time step and applies the optimal input to the plant. We define the CFTOC

$$\min_{u[k]\in\mathcal{U}} \quad \left\|(q_b\bar{\mathbf{R}} + q_c\mathbf{R})\tilde{x}[k+1]\right\|_q + \|r_l u[k]\|_q \tag{21a}$$

$$\text{subject to } \tilde{x}[k+1] = \mathbf{L}x[k+1] - r; \tag{21b}$$

$$x[k+1] = x[k] + \mathbf{B}u[k] + \mathbf{E}w[k] \in \mathcal{X}. \tag{21c}$$

The prediction horizon is chosen equal to one due to the assumption that the battery voltages are slow varying with respect to one sampling time. A longer horizon can be chosen extending this assumption to multiple sampling times. The cost function (21a) is defined using the infinity norm ($q = \infty$), one norm ($q = 1$) or squared two norm ($q = 2$). The tuning parameter $q_b \in \mathbb{R}_{\geq 0}$ defines the importance of balancing, $q_c \in \mathbb{R}_{\geq 0}$ defines the importance of charging and $r_l \in \mathbb{R}_{\geq 0}$ penalizes the actuation of large balancing currents that are related to losses.

The controller (21) is based on the assumption that the capacity of the LV element Q_L is relevant, i.e. not negligible, with respect to the HV elements. In these conditions, it is realistic to assume that the the voltages $v_1, \ldots, v_n$ and v_L vary with similar rates and the balancing and charging problem can be addressed by a single controller. An example is a HEV or EV where the LV bus is connected to a lead-acid battery.

The charging control tends to a voltage regulation problem when the LV auxiliary system does not feature a relevant energy storage element, e.g. when the voltage is stabilized only by a capacitor. Voltage regulation requires a significantly higher bandwidth and sampling rates compared to balancing.

[1]The LV auxiliary system absorbs power such that balancing is possible over time. However, this operation depends on the LV load that is small in some circumstances, e.g. in a parked vehicle. Controllability can be restored with a LV chopper.

The proposed balancing and charging MPC is applicable also in this case. However, the CFTOC (21) can be challenging to solve at fast sampling rates. Thus, we introduce a *decoupled* control strategy that separates balancing and charging. Conceptually, the balancing and charging control problem can be split into two subproblems and solved independently from each other. We define the input $u[k]$ as the sum of two components

$$u[k] = u_b[k] + u_c[k], \tag{22}$$

where $u_b[k] \in \mathbb{R}^n$ is used for balancing and $u_c[k] \in \mathbb{R}^n$ is used for charging without affecting the charge distribution of the HF elements. The component $u_b[k]$ is not allowed to alter the SOC of the LV element between two sampling instants, i.e. $x_L[k+1] = x_L[k]$ (with $i_L = 0\text{A}$).

Proposition 4. *Let* $u_b[k] \in \mathcal{U}_b = \left\{u_b \in \mathbb{R}^n \mid \boldsymbol{R}\tilde{\boldsymbol{B}}u_b = 0_{n+1}\right\}$ *and* $w[k] = 0_2$*, then* $u[k] = u_b[k]$ *yields* $x_L[k+1] = x_L[k]$.

Proof. Multiplying (18) with $\mathbf{R}$, substituting $u[k] = u_b[k] \in \mathcal{U}_b$, and $w[k] = 0_2$ yields $\mathbf{R}(\tilde{x}[k+1] - \tilde{x}[k]) = \mathbf{R}\tilde{\mathbf{B}}u_b$, where the first n components are identically zero for any $u_b \in \mathcal{U}$ and the $n+1$-th component is zero if and only if $\mathbf{R}\tilde{\mathbf{B}}u_b = 0_{n+1}$. □

The component $u_c[k] \in \mathbb{R}^n$ is used for charging without affecting the unbalanced SOC of the HF elements, i.e. $\bar{x}_j[k+1] = \bar{x}_j[k]$ (with $i_H = 0\text{A}$).

Proposition 5. *Let* $u_c[k] \in \mathcal{U}_c = \left\{u_b \in \mathbb{R}^n \mid \bar{\boldsymbol{R}}\tilde{\boldsymbol{B}}u_c = 0_{n+1}\right\}$ *and* $w[k] = 0_2$*, then* $u[k] = u_c[k]$ *yields* $\bar{x}_j[k+1] = \bar{x}_j[k]$.

Proof. The proof is similar to the proof of Proposition 4. □

These results are now used to derive a decoupled control strategy. We define the optimization problem

$$\min_{u[k],u_b[k]\in\mathcal{U}} \quad \left\|q_b\bar{\mathbf{R}}\tilde{x}[k+1]\right\|_q + \|r_l u[k]\|_q \tag{23a}$$

$$\text{subject to } \tilde{x}[k+1] = \mathbf{L}x[k+1] - r; \tag{23b}$$

$$x[k+1] = x[k] + \mathbf{B}u[k] + \mathbf{E}w[k] \in \mathcal{X}; \tag{23c}$$

$$u[k] = u_b[k] + h;\ u_b[k] \in \mathcal{U}_b \tag{23d}$$

$$h \in \mathcal{U}_c;\quad R'\tilde{\mathbf{B}}h = I_{\text{cr}} \tag{23e}$$

The cost function (23a) focuses solely on balancing of the HV elements as charging is taken into account externally. The equality constraints (23b) and (23c) provide the transformed state of the next sampling instant. The total link current is given by (23d), where $u_b[k]$ is reserved for balancing. Similarly, (23e) requires that h is used solely for charging providing the rated charging current I_{cr} to the LV system. The optimization problem (23) is feasible under the condition that the required charging current $I_{\text{cr}} > 0$ does not exceed the maximum deliverable current, i.e.

$$I_{\text{cr}} \leq 1_n' \left[\frac{V_1}{V_L} I_{1,\text{max}}, \ldots, \frac{V_n}{V_L} I_{\text{n,max}}\right]'. \tag{24}$$

The optimization problem (23) defines the vectors $u_b[k]$ and h that define the control law

$$u[k] = u_b[k] + h\rho[k]. \tag{25}$$

The coefficient $\rho[k] \in [0, 1]$ is used to define the charging current $u_c[k] = h\rho[k]$, e.g. with a proportional controller. A block diagram is depicted in Fig. 4(b).

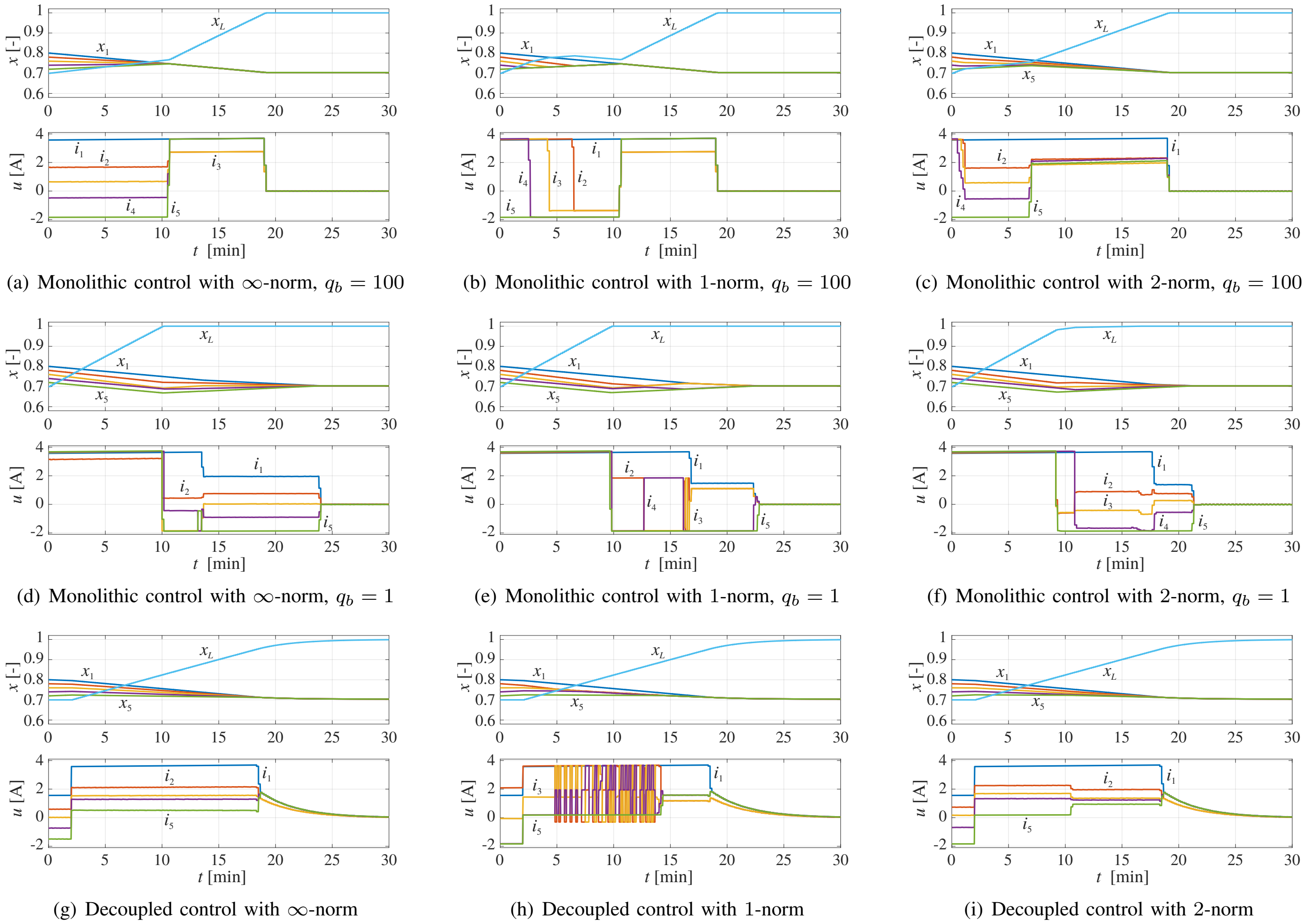

(a) Monolithic control with ∞-norm, $q_b = 100$ (b) Monolithic control with 1-norm, $q_b = 100$ (c) Monolithic control with 2-norm, $q_b = 100$

(d) Monolithic control with ∞-norm, $q_b = 1$ (e) Monolithic control with 1-norm, $q_b = 1$ (f) Monolithic control with 2-norm, $q_b = 1$

(g) Decoupled control with ∞-norm (h) Decoupled control with 1-norm (i) Decoupled control with 2-norm

Fig. 5. Software-in-the-loop validation: balancing and charging using monolithic MPC (21) and decoupled MPC (23) with the tuning parameters $q_c = 1$ and $r_l = 0$; the initial state $x(0) = [0.80, 0.78, 0.76, 0.74, 0.72, 0.70]'$; cell capacities $\mathbf{Q} = \mathrm{diag}[12, 9, 9, 12, 12, 3]'$Ah; and input limits $I_{\text{k,max}} \approx 3.8$A, and $I_{\text{k,min}} \approx -1.8$A (the exact limits vary with the cell voltages [15])

By design, the controller (25) is always feasible since $\mathcal{U}$ is convex and $u[k]$ lies on the straight between $u_b[k] \in \mathcal{U}$ and $u_b[k] + h \in \mathcal{U}$. Furthermore, the affine equation (25) is trivial to execute at fast sampling rates, e.g. $T_s \ll 1$ms. This property is made possible by reserving the subset of the link currents h for charging. However, the instantaneous charging load $h\rho[k]$ is not known at the time of solving the CFTOC (23) that leads to instances where the links are not fully utilized. Hence, the monolithic CFTOC (21) approach is generally preferable over CFTOC (23) if both approaches are computationally viable.

It is noted that the optimization problem (23) requires bidirectional links for balancing. Otherwise, (23) yields a vector $u_b[k] = 0_n$ and the resulting controller (25) will only supply power to the LV link. Balancing is still possible with unidirectional links and small LV storage element for example defining a charging vector that tends to balance the HV elements. However, the resulting balancing operation is load dependent and therefore not treated in this text.

VI. Evaluation

The BB-APM is validated using the monolithic and decoupled control using a software-in-the-loop (SiL) platform and an experimental test bench. The SiL platform executes the original control code and emulates the LV and HV batteries and the balancing electronics using Matlab-Simulink high fidelity models [15], [29]. The experimental setup consists of a reconfigured LT DC2100A demo board that is interfaced with a TI F28377D control DSP as shown in Fig. 6(a). The original board uses a cell-to-stack topology [29] that has been modified into a BB-APM with LV energy storage element. The HV and LV batteries are custom build stacks using Panasonic NCR 18650 cells. Both batteries have a similar voltage rating due to the existing transformer winding ratios of the bidirectional flyback converter links. Each flyback module operates in critical mode with pulse frequency modulation (PFM). PFM leads to maximum and minimum link currents that depend on the cell voltages V_j [15]. They are slow varying within limited intervals and taken into account throughout testing.

The BB-APM is tested using both monolithic and decoupled control. The results and performance metrics are shown in Fig. 5 and Table II. The time to balance (t2b) and time to charge (t2c) are the times necessary such that $x[k] \in \mathcal{X}_b$ and $x[k] \in \mathcal{X}_c$, respectively within 1% tolerance. The energy-loss to balance and charge (e2bc) is the energy lost due to

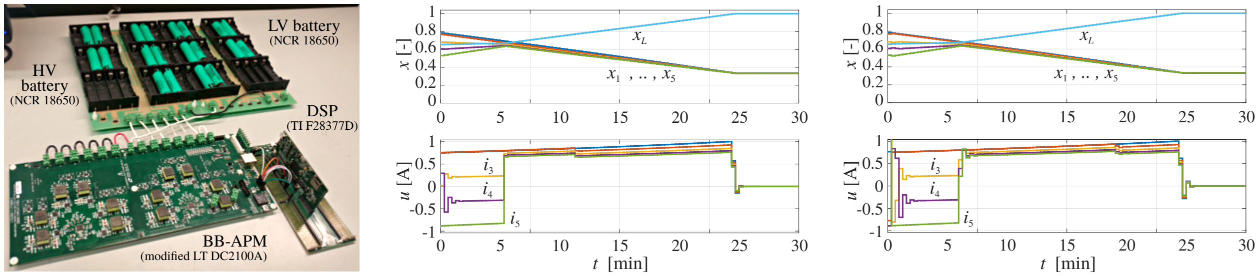

(a) Experimental test bench (b) Software-in-the-loop results (c) Experimental results

Fig. 6. Experimental validation: balancing and charging using monolithic control using $q_b = 10$, $q_c = 1$, $r_l = 0$ and the initial state $x(0) = [0.784, 0.768, 0.681, 0.606, 0.531, 0.654]'$, $\mathbf{Q} = \text{diag}[6, 6, 6, 6, 6, 6]'$Ah, $I_{\text{k,max}} \approx 0.9$A, and $I_{\text{k,min}} \approx -0.9$A (the exact limits vary with the cell voltages)

link efficiency for achieving $x[k] \in \mathcal{X}_b \cap \mathcal{X}_c$. Furthermore, the control execution time T_x is measured that is the CPLEX solver time for the CFTOC (21) and CFTOC (23), and the time to compute the control law (25) (and feedback controller).

Monolithic control optimizes both charging and balancing simultaneously. The tuning of the cost function can prioritize balancing over charging (Fig. 5(a), Fig. 5(b), and Fig. 5(c)) or vice-versa (Fig. 5(d), Fig. 5(e), and Fig. 5(f)). The same figures also depict the effect of different types of cost functions: ∞, 1, or squared 2 norm. The control trajectories depend on the type of cost function. Compared to the quadratic cost function, the linear ones tend to faster variations of the link current. In particular, the 1 norm is prone to repeated charging and discharging (microcycling) of the cells that results in increased losses due to the link efficiency [29]. The squared 2 norm effectively avoids this behavior and tends to a single point of convergence of the HV cell SOC and approximately constant balancing link currents (at given charging currents) that minimize losses [29]. On the other hand, the squared 2 norm yields a quadratic program that requires about 7 times the processing time compared to the linear programs that result from the 1 norm and ∞ norm cost functions.

The decoupled control identifies two control inputs, where the first handles balancing and the second can be manipulated for charging. The latter can be manipulated with the same or a higher sampling frequency. This ability is shown executing the charging control at 10 times the sampling frequency of the balancing control. The decoupled control is shown in Fig. 5(g), Fig. 5(h), and Fig. 5(i). At $t = 0$min, only balancing control is active (setting $\rho[k] = 0$) and charging control (saturated gain) is activated at $t = 2$min. During this interval, the balancing links are not fully utilized that leads to an increased t2c and/or t2b. Similar to monolithic control, the 1 norm cost function (Fig. 5(h)) leads to microcycling and an increased e2bc compared to the quadratic cost function. The execution times of the decoupled CFTOC (23) and monolithic CFTOC (21) are similar. However, the decoupled CFTOC issues the control law (25) that is approximately 10^6 times faster to execute than either strategies. Therefore, decoupled control can achieve a high charging bandwidth since the charging control is trivial to execute at high sampling frequencies.

The experimental test bench is used to validate the practical feasibility of the proposed MPC control strategies. The test bench only supports slow sampling frequencies (a limitation of the DC2100A demo board). Hence, the experimental testing focuses on monolithic control. The results are shown and compared to SiL results in Fig. 6. Both results show a good match in the same conditions (parameters and initial conditions). The experimental results show a minor increase of overshoots of the link power since the rated cell capacity is used for control. In practice, the cell capacity varies and it can be fine-tuned via capacity estimation techniques (e.g. [22]) that are not discussed in this paper due to shortness.

VII. Conclusion

This research proposes the integration of the auxiliary power module (APM) and redistributive balancing hardware of a high-voltage battery or supercapacitor pack. The resulting battery-balancing APM (BB-APM) has a similar complexity than other nondissipative balancing topologies and is projected to make redistributive balancing competitive for electric vehicles and some plug-in hybrids using the specific power electronic and battery cost targets from 2020.

The BB-APM is modeled and the balancing and charging problems are formally defined. The resulting control problems are addressed with two model predictive control (MPC) strategies that solve a convex optimization problem at each time step. The *monolithic* control solves both the balancing and charging control subproblems simultaneously. This control is generally preferred since it solves for the global optimum with respect to a quadratic or linear cost function. However,

Table II
Control performance metrics

Case of Fig. 5	**t2b**	**t2c**	**e2bc**	T_x
Monolithic control: CFTOC (21)				
∞-norm, $q_b = 100$	10.7min	18.8min	1.45Wh	0.8ms
1-norm, $q_b = 100$	10.7min	18.8min	1.75Wh	0.8ms
2-norm, $q_b = 100$	19.0min	18.8min	1.34Wh	5.7ms
∞-norm, $q_b = 1$	22.2min	9.8min	1.69Wh	0.8ms
1-norm, $q_b = 1$	20.5min	9.5min	1.90Wh	0.8ms
2-norm, $q_b = 1$	19.2min	10.3min	1.66Wh	5.7ms
Decoupled control: CFTOC (23), control law (25)				
∞-norm	16.3min	21.5min	1.19Wh	1.1ms, 20.9ns
1-norm	15.2min	21.5min	1.25Wh	1.4ms, 21.1ns
2-norm	16.0min	21.5min	1.20Wh	5.9ms, 29.5ns

this control approach requires a low-voltage energy storage element, e.g. a lead-acid battery in an electric vehicle. Without storage, the charging subproblem tends to voltage control of the LV link with significantly faster sampling requirements. Hence, a *decoupled* formulation is proposed that solves the balancing problem at a slow sampling rate and issues a charging control law that is 10^6 times faster to execute.

The control strategies are validated using a software-in-the-loop (SiL) platform that emulates the LV and HV batteries and the balancing electronics with high fidelity models. The control strategies are validated for a range of linear and quadratic cost functions and performance metrics are computed for each case. In comparison, quadratic cost functions yield the lowest losses to achieve the control targets at the cost of a higher computational burden. In further work, a dedicated BB-APM hardware platform will be developed.

VIII. Acknowledgments

The author thanks Prof. Ali Emadi for the valuable discussions and Lucas McCurlie for his support during testing.

References

[1] A. Affanni, A. Bellini, G. Franceschini, P. Guglielmi, and C. Tassoni, "Battery choice and management for new-generation electric vehicles", *IEEE Trans. Ind. Electron.*, vol. 52, pp. 1343–1349, 2005.

[2] S. M. Lukic, J. Cao, R. C. Bansal, F. Rodriguez, and A. Emadi, "Energy storage systems for automotive applications", *IEEE Trans. Ind. Electron.*, vol. 55, pp. 2258–2267, 2008.

[3] J. Cao, N. Schofield, and A. Emadi, "Battery balancing methods: A comprehensive review", in *Vehicle Power and Propulsion Conference (VPPC)*, 2008.

[4] N. H. Kutkut, H. L. N. Wiegman, D. M. Divan, and D. W. Novotny, "Charge equalization for an electric vehicle battery system", *IEEE Trans. Aerosp. Electron. Syst.*, vol. 34, pp. 235–246, 1998.

[5] ——, "Design considerations for charge equalization of an EV battery system", *IEEE Trans. Ind. Appl.*, vol. 35, pp. 28–35, 1999.

[6] D. Andrea, *Battery management systems for large lithium ion battery packs*. Artech House, 2010.

[7] C. R. Birkl, D. F. Frost, A. M. Bizeray, R. R. Richardson, and D. A. Howey, "Modular converter system for low-cost off-grid energy storage using second life li-ion batteries", in *Global Humanitarian Technology Conference (GHTC)*, 2014.

[8] C. S. Moo, Y. C. Hsieh, and I. S. Tsai, "Dynamic charge equalisation for series-connected batteries", *IEE Proceedings Electric Power Applications*, vol. 150, pp. 501–505, 2003.

[9] M. Tang and T. Stuart, "Selective buck-boost equalization for series battery packs", *IEEE Trans. Aerosp. Electron. Syst.*, vol. 36, pp. 201–211, 2000.

[10] M. Preindl, C. Danielson, and F. Borrelli, "Performance eval. of battery balancing hardware", in *European Control Conference (ECC)*, 2013.

[11] Electrical and Electronics Technical Team, "Electrical and electronics technical team roadmap", U.S. DRIVE, Roadmap, 2013.

[12] R. Hou, P. Magne, B. Bilgin, and A. Emadi, "A topological evaluation of isolated dc/dc converters for auxiliary power modules in electrified vehicle applications", in *Applied Power Electronics Conference and Exposition (APEC)*, 2015.

[13] R. Hou and A. Emadi, "Applied integrated active filter auxiliary power module for electrified vehicles with single-phase onboard chargers", *IEEE Trans. Power Electron.*, vol. PP, pp. 1–1, 2016.

[14] B. Nykvist and M. Nilsson, "Rapidly falling costs of battery packs for electric vehicles", *Nature Climate Change*, vol. 5, pp. 329–332, 2015.

[15] L. McCurlie, M. Preindl, P. Malysz, and A. Emadi, "Simplified control for redistributive balancing systems using bidirectional flyback converters", in *Transportation Electrification Conference and Expo (ITEC)*, 2015.

[16] C. Danielson, F. Borrelli, D. Oliver, D. Anderson, M. Kuang, and T. Phillips, "Balancing of battery networks via constrained optimal control", in *American Control Conference (ACC)*, 2012.

[17] K. Thomas, J. Newman, and R. Darling, "Mathematical modeling of lithium batteries", in *Advances in Lithium-Ion Batteries*, W. A. van Schalkwijk and B. Scrosati, Eds., 2002, pp. 345–392.

[18] G. Sikha, R. E. White, and B. N. Popov, "A mathematical model for a lithium-ion battery/electrochemical capacitor hybrid system", *J Electrochem Soc*, vol. 152, A1682–A1693, 2005.

[19] H. He, R. Xiong, X. Zhang, F. Sun, and J. Fan, "State-of-charge estimation of the lithium-ion battery using an adaptive extended kalman filter based on an improved thevenin model", *IEEE Trans. Veh. Technol.*, vol. 60, pp. 1461–1469, 2011.

[20] J. Kim and B. H. Cho, "SoC estimation and SoH prediction of a li-ion degraded battery based on an ekf combined with a per-unit system", *IEEE Trans. Veh. Technol.*, vol. 60, no. 9, pp. 4249–4260, 2011.

[21] M. Shahriairi and M. Farrokhi, "Online state of health estimation of vrla batteries using state of charge", *IEEE Trans. Ind. Electron.*, vol. 60, pp. 191–202, 2013.

[22] P. Malysz, R. Gu, J. Ye, H. Yang, and A. Emadi, "State-of-charge and state-of-health estimation with state constraints and current sensor bias correction for electrified powertrain vehicle batteries", *IET Electr. Syst. Transp.*, vol. 6, no. 2, pp. 136–144, 2016.

[23] B. Bilgin, P. Magne, P. Malysz, Y. Yang, V. Pantelic, M. Preindl, A. Korobkine, W. Jiang, M. Lawford, and A. Emadi, "Making the case for electified transportation", *IEEE Trans. Transport. Electrific.*, vol. 1, pp. 4–17, 2015.

[24] F. Baronti, R. Roncella, and R. Saletti, "Performance comparison of active balancing techniques for lithium-ion batteries", *J. Power Sources*, vol. 267, pp. 603–609, 2014.

[25] C. Danielson, F. Borrelli, D. Oliver, D. Anderson, and T. Phillips, "Constrained flow control in storage networks: Capacity max. and balancing", *Automatica*, vol. 49, pp. 2612–2621, 2013.

[26] K. M. Lee, Y. C. Chung, C. H. Sung, and B. Kang, "Active cell balancing of li-ion batteries using lc series resonant circuit", *IEEE Trans. Ind. Electron.*, vol. 62, pp. 5491–5501, 2015.

[27] Z. Zhang, H. Gui, D. J. Gu, Y. Yang, and X. Ren, "A hierarchical active balancing architecture for lithium-ion batteries", *IEEE Trans. Power Electron.*, vol. PP, pp. 1–1, 2016.

[28] J. G. Pinto, V. Monteiro, H. Goncalves, and J. L. Afonso, "Onboard reconfig. battery charger for electric vehicles with traction-to-auxiliary mode", *IEEE Trans. Veh. Technol.*, vol. 63, pp. 1104–1116, 2014.

[29] L. McCurlie, M. Preindl, and A. Emadi, "Fast model predictive control for redistributive lithium ion battery balancing", *IEEE Trans. Ind. Electron.*, vol. 64, pp. 1350–1357, 2016.

Matthias Preindl (S'12-M'15) received the B.Sc. degree in electrical engineering (*summa cum laude*) from the University of Padua, Padua, Italy, the M.Sc. degree in electrical engineering and information technology from ETH Zurich, Zurich, Switzerland, and the Ph.D. degree in energy engineering from the University of Padua, in 2008, 2010, and 2014, respectively. He was an R&D Engineer of Power Electronics and Drives at Leitwind AG, Sterzing, Italy (2010-2012), a Post Doctoral Research Associate with the McMaster Institute for Automotive Research and Technology, McMaster University, Hamilton, ON, Canada (2014-2015), and a Sessional Professor in the Department of Electrical and Computer Engineering, McMaster University (2015). He is currently an Assistant Professor in the Department of Electrical Engineering, Columbia University in the City of New York, NY, USA. He received the Career Award of the Futura Foundation in South Tyrol, Italy and the CAREER Award of the US National Science Foundation (NSF) in 2016 and 2017, respectively.